

# Simulated Photometry of Objects in Cislunar Orbits

Phan Dao

*Air Force Research Laboratory, Space Vehicles Directorate*

**Kristen Haynes, Victoria Frey, Cory Hufford,**

**Kyle Schindler, Tamara Payne, and Jeffrey Hollon**

*Applied Optimization*

## CONFERENCE PAPER

### ABSTRACT

Lately, there has been an increased global interest in sending satellites to the Moon. As more objects enter the cislunar domain, cislunar Space Domain Awareness (SDA) is becoming a necessity. Since most SDA is currently concerned with objects from Low Earth Orbit (LEO) to Geosynchronous Earth Orbit (GEO), much work has already been done to study the photometry of objects in these orbits. Some of this knowledge can be applied to the study of cislunar objects.

Like objects in GEO, imagery of cislunar objects will be unresolved from ground-based sensors or space-based sensors due to the distances involved. Additionally, objects orbiting the Moon or the L1 or L2 Lagrange points will repeat a pattern of photometric behavior once per lunar cycle, which can be used to predict future behavior. However, unlike GEO objects, which repeat a pattern of photometric behavior over the diurnal cycle, there is a wider variety of cislunar orbital shapes causing a wider variety of photometric behavior. Also, cislunar space is a much larger volume of space so tracking and predicting the behavior of cislunar targets is a more complicated problem.

Simulating photometry for a variety of cislunar scenarios will be useful to help predict behavior of future objects flown in cislunar space. We have simulated various cislunar scenarios using NASA's General Mission Analysis Tool (GMAT). Photometry for these orbits were then simulated using the Satellite Visualization and Signature Tool (SVST) for targets of differing sizes. The sensor for these simulations was placed either on Earth or on the Moon to get a perspective of how the photometry and observability of the target changes with the sensor location.

With these simulations, we are able to analyze the photometry of an object in all stages of a cislunar orbit (i.e., Earth orbit, transfer, lunar/L1/L2 orbit). We are also able to specify expected signal strength for typical spacecraft and interference noise based on the geometry of the sensor, target, the Moon, and the Sun. This paper will describe the different orbits studied, present the simulation results with special attention to cislunar object brightness ranges, photometric signature patterns, and observability.

## 1. INTRODUCTION

Since the beginning of the Space Age and the launch of the first artificial satellite, optical measurements have been one of the main approaches of finding and keeping track of Resident Space Objects (RSOs). Until recent times, the challenge of space traffic management has been limited to monitoring and cataloging RSOs up to geosynchronous and geocentric, super-synchronous distances. Furthermore, optical sensor systems have been designed with sufficient sensitivity to detect reasonably-sized objects at GEO and super-GEO distances, and these systems have had coverage to maintain robust custody of objects in GEO and super-GEO. Routine optical measurements of

photometric signatures (light curves) are conducted by telescopes located around the globe. Fig. 1 shows a sample GEO light curve of DIRECTV-10 recorded over a period of 10 hours on 25 Feb 2013. The abscissa shows the signed Longitudinal Phase Angle (LPA) of the space object during the observation session. The ordinate is the satellite brightness in magnitudes as measured in the Johnson-Cousins R spectral band. Further analysis of the light curves infers the satellite's status; for example, the solar panel was offset from solar longitude by approximately two degrees. The GEO light curve qualitatively repeats itself every 24 hours. For active and attitude-controlled satellites, techniques for analyzing photometric data take into account the mode of attitude control relative to the directions to the Sun and Earth's nadir [1].

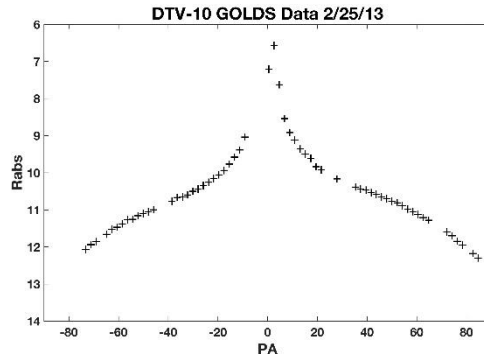


Fig. 1. Light Curve of Satellite DIRECTV-10 (NORAD 31862) Collected by the Air Force Research Laboratory on 25 Feb 2013

As spacefaring countries expand their objectives to explore [2] or return to the Moon [3] and advance further to nearby planets such as Mars, many concepts of a lunar parking orbit have been considered to support future exploration and exploitation of space. In the Moon's sphere of influence, the orbits around the Earth-Moon L1 and L2 Lagrange points have been considered and used by several space programs [4]. While the satellite owners have intimate knowledge of their space assets, other countries do not necessarily have access to the same information in a timely manner, and no one agency has custody of these cislunar RSOs. An important question is whether we can have an independent capability to maintain custody and manage traffic in translunar and cislunar space. As far as optical sensors are concerned, this paper begins to address the observational capability required to monitor and keep track of space objects in cislunar space. In this context, the term cislunar refers to orbits that exist in the framework of the Earth-Moon three body problem. Since L1 and L2 cislunar orbits are in the forefront of current space activities, one of the simulations of this study will focus on a halo orbit around the L2 Lagrange point. With the simulation of photometric signatures, our goal is to help assess the contribution of ground optical sensors to the monitoring of cislunar RSOs. To estimate the range of expected apparent visual magnitudes, RSO pose and illumination geometry are critical elements for the simulations. Reflected brightnesses depend on the physical attributes of the RSO. Signature simulation tools will be used to account for differences in attitude control mode, distances, and illumination angles. A relevant selection of satellite solid models will be used.

The main photometric measurement of a sun-lit space object is reported in stellar magnitude. The apparent magnitude  $m_{app}$  of a satellite is calculated as follows.

$$m_{app}(v) = M_{sun}(v) - 2.5 \log \left( \frac{F_{app}(v)}{F_{sun}(v)} \right) \quad (1)$$

The variable  $v$  is the optical band of the sensor, and for this work, we have chosen the Johnson-Cousins R filter in the visible spectrum.  $M_{sun}$  is the Sun's magnitude in the R band.  $F_{app}$  is the flux of the space object, and  $F_{sun}$  is the solar flux in the R band; both are scaled appropriately for distance. The ratio of lunar to GEO distance is approximately an order of magnitude. Therefore, the RSO's flux  $F_{app}$  is 100 times smaller, so the apparent

magnitude should be increased by 5 (dimmer) for lunar distance. However, the light curve of a maintained GEO can vary by as much as 6 - 7 magnitudes as seen in Fig. 1. We would like to know how a larger distance and a different set of geometric factors would change the observability of a satellite in translunar and cislunar orbits. We would like to find out whether the light curve would repeat itself, and if it does, we want to know whether it will have an apparent periodicity longer than in GEO, i.e., a diurnal cycle. We are interested in revealing not just the range of brightnesses, but also the light curves that may be observed if future satellites are in a translunar/lunar orbit, such as the Chandrayaan-2 or a translunar/cislunar orbit such as the Chang'e-4. Realistic satellite solid models and attitude control modes will be used for this purpose. In addition to simulating the measurements from the ground-based telescope at the Air Force Research Laboratory's Starfire Optical Range (SOR), we also simulate the light curves as seen from a hypothetical site on the Moon.

## 2. METHODOLOGY AND SIMULATION TOOLS

### 2.1 GENERAL MISSION ANALYSIS TOOL

To simulate the trajectory of cislunar objects, we used NASA's General Mission Analysis Tool (GMAT) (version R2018a). This software allows the user to set the trajectory at an initial epoch and numerically propagate the orbit. For example, the user could provide a set of orbit elements or a state vector to define the orbit. Several initial parameters can be set to define the attitude, mass, fuel tanks, and power system of the spacecraft. The user can also edit the propagator. In the propagator, the primary body of the force model can be set and different gravity models can be used for the primary body. Atmosphere models and point masses can be added to the force model to help create a more realistic orbit. The numerical integrator type used for the propagator can be set by the user as well to meet desired stabilities and accuracies. For geocentric orbits, we used the Joint Earth Gravity Model-2 (JGM-2) for Earth with the Moon and Sun as point masses. The MSISE90 atmospheric model was used for the Chandrayaan-2 simulation for the LEO portion. For lunar orbits, Earth, the Moon, and the Sun were all treated as point masses. The authors realize that because of the simplifying assumptions listed above that the orbits generated are notional and only meant for geometric analysis of photometric light curves from cislunar objects.

After setting the initial parameters, the orbit trajectory can be propagated forward and maneuvers can be applied to the spacecraft to change the trajectory. Maneuvers can be applied manually (i.e., the user can provide the change in velocity,  $\Delta v$ , to apply at a specified time) or the user can define a target (e.g., target location, eccentricity, etc.) and allow the software to solve for the  $\Delta v$  that will allow the spacecraft to achieve that target within a specified error bound. A maneuver can be performed using an impulsive burn or finite burn. We used impulsive burns for each maneuver in our simulations for the sake of simplicity.

### 2.2 SIMULATION TOOL METHODOLOGY

After the cislunar orbits were designed in GMAT, the orbital information was imported into the Satellite Visualization and Signature Tool (SVST) (version 8.3.51) in order to simulate the light curves. A Computer-Aided Design (CAD) satellite model was used as the target. The target's attitude was Earth-nadir facing with the solar panels tracking the Sun. The sensor was positioned at either the SOR in New Mexico, USA or on the Earth-facing side of the Moon. The sensor was set to have a flat-top 300-1100 nm optical transmission, with a filter response curve similar to the Johnson-Cousins R spectral filter<sup>1</sup>, and an 'AndorQE'<sup>2</sup> Quantum Efficiency (QE). To render the simulated images, the best Instantaneous Field of View (IFOV) angle per frame option was used, and the pristine image dimensions were set to a resolution of 256x256. Both solar illumination and lunar illumination were selected as radiometric contributors.

---

<sup>1</sup> 'JohnsonRed.dat' is a file included with SVST that can be used to represent a Johnson red filter. It is assumed that it is representative of a Johnson-Cousins R filter.

<sup>2</sup> 'AndorQE.dat' is a file included with SVST that can be used to represent the QE of a Charge-Coupled Device (CCD). It is assumed that it represents the QE of a typical Andor sensor.

During simulations, we noticed some limitations of SVST, particularly in relation to lunar orbiters. SVST automatically flags some observations considered to be invalid; however, it does not catch all possible cases of invalid observations. We have identified that SVST flags observations as invalid when the Earth is between the sensor and target and when no light from the target can be detected by the sensor. SVST flags these observations by returning a magnitude of 30. The invalid cases we have identified that SVST does not handle are when

- The sensor is in sunlight.
- The satellite is behind the Moon from the sensor's point-of-view (lunar occultation).
- The satellite is directly in front of the Moon from the sensor's point-of-view (sensor saturation).

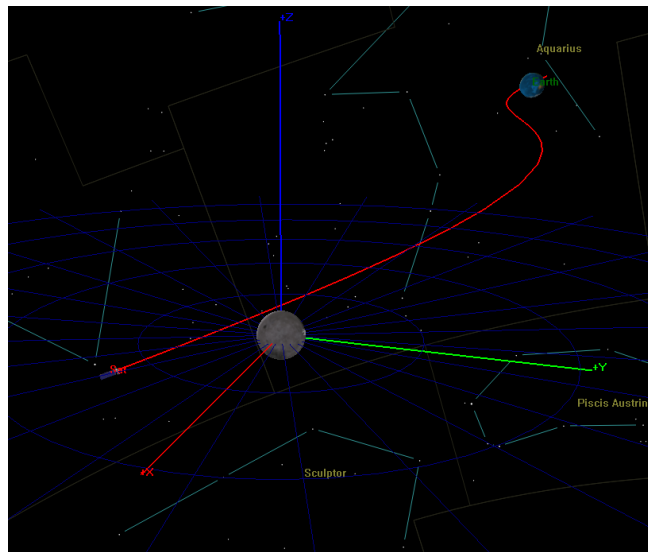
In order to improve simulation realism, a post-processing script was written to flag invalid observations caused by these cases that SVST does not handle. In addition to these three cases, our post-processing script determines when

- The satellite is in the Earth or Moon's shadow.
- The satellite is in the Sun's exclusion zone (set to  $20^\circ$  from limb). This also results in sensor saturation.
- The satellite is in the Earth's exclusion zone (set to  $5^\circ$  from limb).
- The satellite is in the Moon's exclusion zone (set to  $5^\circ$  from limb).

Ideally, object's detectability can be determined with a signal to noise ratio. Because we don't use a sensor model and background noise is not available, the exclusion zones are implemented to determine when the object is not detectable because the light of sight is too close to a source of high background. All invalid observations are flagged or removed in the plots of our simulation results. We did not set a limiting magnitude for the sensors, so no observations are flagged or removed for being too dim to detect.

### 3. TRANSLUNAR AND TRANSEARTH TRAJECTORIES

Fig. 2 shows three typical translunar trajectories that leave a low altitude perigee to arrive at the Moon just before injection into a lunar or cislunar orbit. The three scenarios were designed in GMAT. The design is such that the spacecraft's transit times from the three scenarios are 35 hours, 72 hours, and 5 days. The object's coordinates are used with SVST to estimate its brightness in magnitudes.



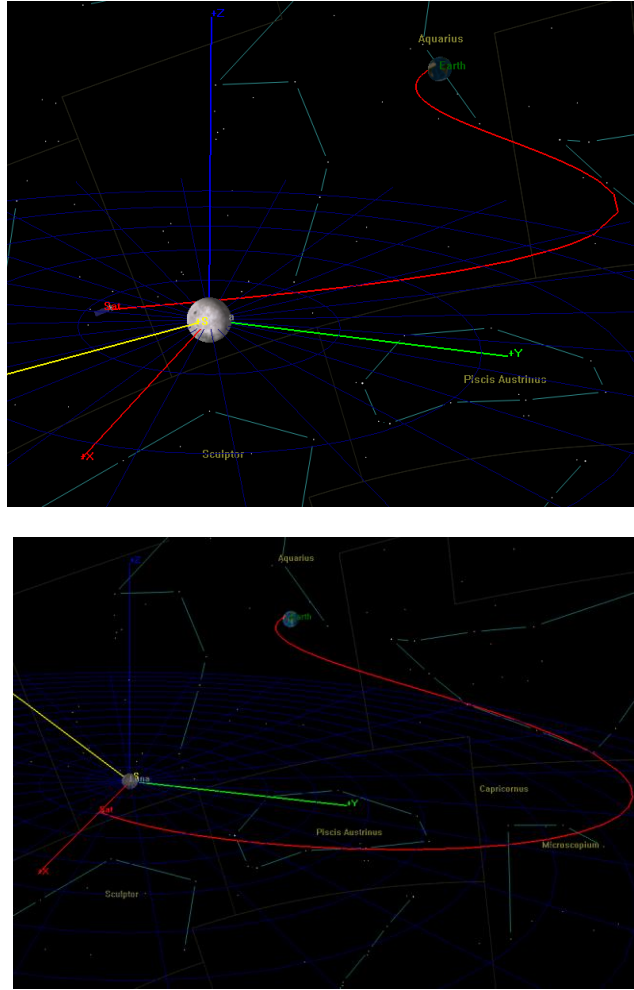


Fig. 2a. Top: Luna 35-Hour Translunar Orbit; Middle: Apollo 72-Hour Translunar Orbit; Bottom: 5-Day Translunar Orbit

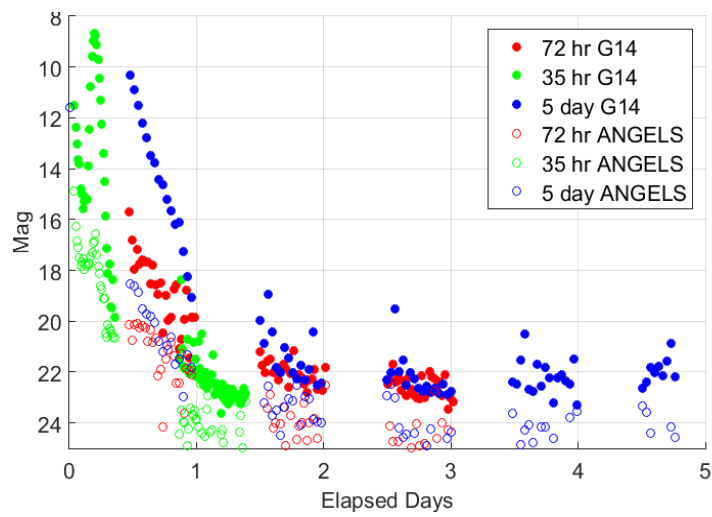


Fig. 3b. R-band Magnitudes for the Orbits in Fig. 2a for an SOR telescope

#### 4. CHANDRAYAAN-2 TRAJECTORY

Since cislunar orbits have become of interest, we decided to simulate a real life cislunar orbit. We chose to simulate Chandrayaan-2 because many details about its orbit were made public online. To simulate the orbit of Chandrayaan-2, the initial orbit parameters were estimated and provided to GMAT. The GMAT simulation began on 23 Jul 2019 22:30 UTC, slightly after launch, so the satellite would already be in orbit [5]. The Keplerian orbital elements were used to define the initial orbit. Based on the initial apogee and perigee, the eccentricity (ECC) and semi-major axis (SMA) were calculated [5]. The remaining elements (such as inclination (INC)) were altered such that the transfer orbit would connect with the Moon's trajectory later in the orbit. The dry mass of Chandrayaan-2 was also specified as 1,308 kg [6].

This simulation could only estimate the true orbit of Chandrayaan-2 because not all of the orbital information was available online, thus there are some slight differences between our simulation and the real scenario. The dates and the relevant orbital parameters for each phase of the simulated orbit are given in Table 1.

A geocentric view of the simulated orbit is shown in Fig. 4. Each phase of the orbit is plotted in the same color used for that orbit phase's row in Table 1. The inclined orbit of the Moon is plotted in light grey. The progressively more eccentric geocentric orbits (A-E) can be seen in the figure. Notice how the satellite's orbit extends past the Moon's trajectory before turning around and orbiting the Moon.

Table 1. Information about the Simulated Orbit for Chandrayaan-2

ID	Type	Start (UTC)	Stop (UTC)	Period (hr)	ECC	INC (°)	Apoapsis (km)	Periapsis (km)	Source
A	Earth	7/23/2019 22:30	7/25/2019 15:39	~13.72	0.773	13.432	45203.44	175.015	[7]
B	Earth	7/25/2019 15:39	7/29/2019 22:50	~17.2	0.804	13.432	54668.75	236.198	[8]
C	Earth	7/29/2019 22:50	8/1/2019 22:48	~23.99	0.843	13.425	71469.22	224.406	[9]
D	Earth	8/1/2019 22:48	8/5/2019 22:28	~31.89	0.871	13.391	89146.59	183.703	[10]
E	Earth	8/5/2019 22:28	8/13/2019 10:59	~60.17	0.916	13.361	143018.1	192.587	[11]
F	Transfer	8/13/2019 10:59	8/20/2019 14:34	N/A	N/A	N/A	N/A	N/A	[12], [13]
G	Lunar	8/20/2019 14:34	8/27/2019 10:42	~6.31	0.539	61.587	4428.034	99.873	[14]
H	Lunar	8/27/2019 10:42	8/29/2019 15:24	~3.18	0.244	60.407	1412.734	123.895	[15]
I	Lunar	8/29/2019 15:24	8/31/2019 14:32	~2.05	0.015	67.07	181.109	123.705	[16]
J	Lunar	8/31/2019 14:32	9/16/2019 15:18	~2.01	0.006	66.835	138.871	118.137	[17]

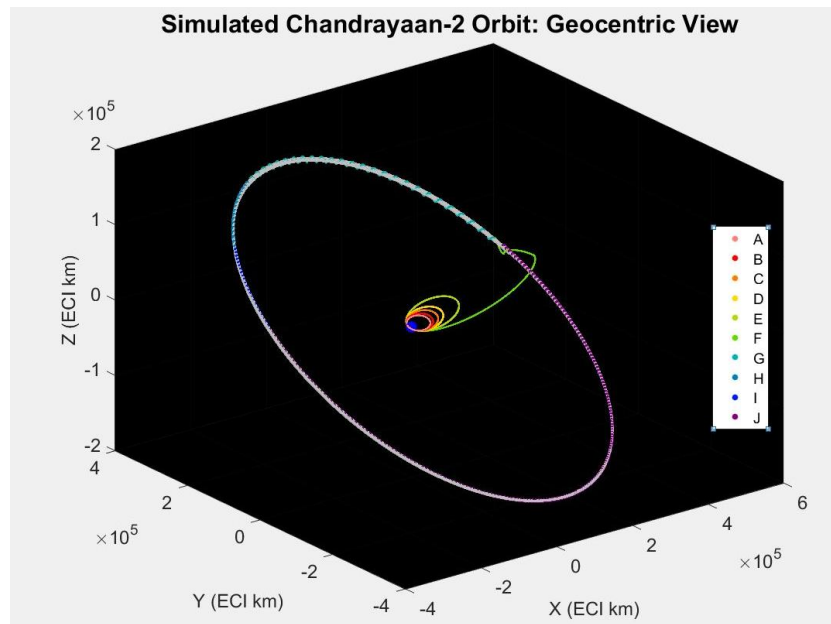


Fig. 4. Geocentric View of the Simulated Chandrayaan-2 Orbit (Earth is Not to Scale)

A selenocentric view of the orbit was also plotted for the end of the transfer orbit and all of the lunar orbit phases of the simulated Chandrayaan-2 orbit. This view of the orbit is shown in Fig. 5. The progressively less eccentric orbit about the Moon is evident in this plot as the orbit progresses from orbit G through orbit J.

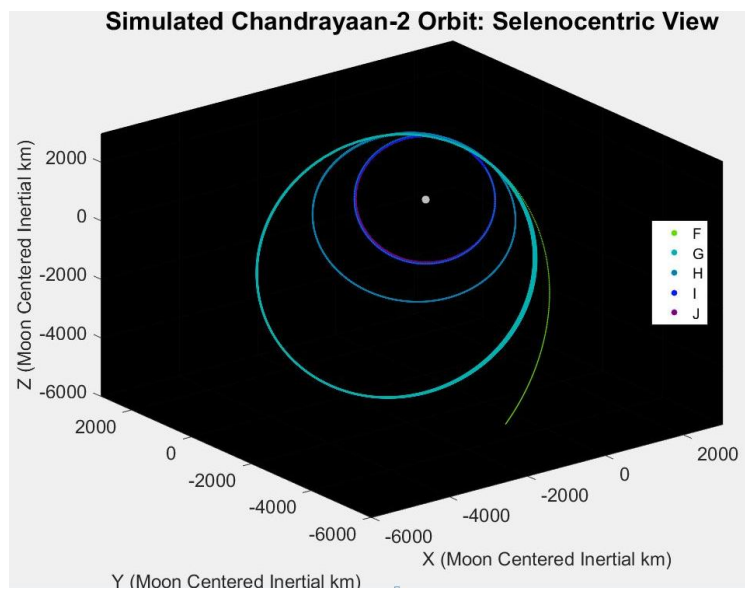


Fig. 5. Selenocentric View of the Simulated Chandrayaan-2 Orbit (Moon is Not to Scale)

Once the orbit was simulated in GMAT, we were able to simulate light curves using SVST. A Galaxy-14, Earth-nadir facing, model was used as a surrogate for the Chandrayaan-2 spacecraft. This model does not look like Chandrayaan-2; however, we do not have access to a satellite model similar to Chandrayaan-2. Simulations were done for an Earth ground-based sensor at SOR and a Moon ground-based sensor on the Earth-facing side of the Moon.

For the full simulation (spanning approximately 56 days), we simulated the light curve with a cadence of five minutes. Magnitude versus date for the full simulation for the SOR observer and Moon-based observer are plotted in Fig. 6 and Fig. 7, respectively. In each plot, valid observations are represented as black dots. If the satellite was below the horizon or the sensor was in sunlight, no marker is displayed. If an observation was invalid for any other reason, it was plotted with a different color and marker than the valid observations (refer to the plot legends for why the observation was considered invalid).

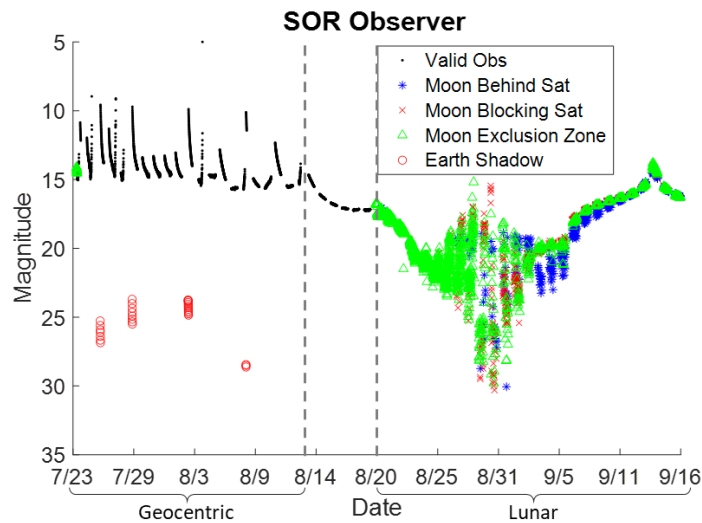


Fig. 6. Magnitude versus Date for Full Chandrayaan-2 Simulation for SOR Sensor

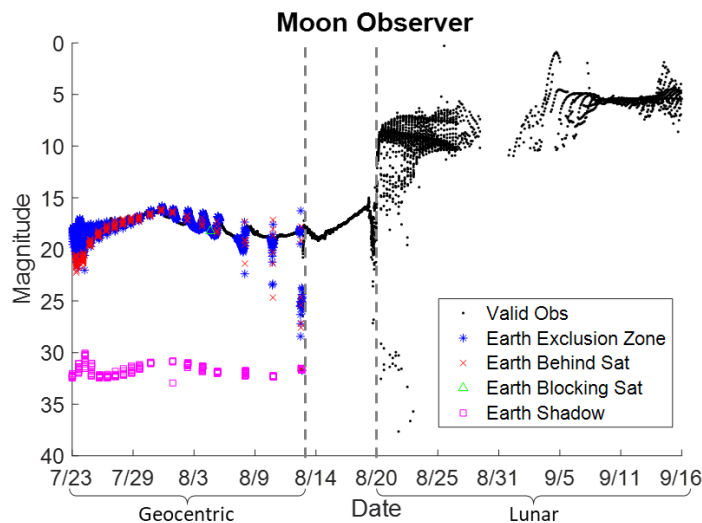


Fig. 7. Magnitude versus Date for Full Chandrayaan-2 Simulation for Lunar Sensor

For individual dates' light curves, a higher cadence was used (approximately 30 seconds) to get a higher resolution of the satellite's behavior on that date. We did not simulate all 56 days at this higher cadence due to time constraints, but did simulate nights from a variety of phases of the orbit.

On 31 July 2019, the satellite was in geocentric orbit C (refer to Table 1). This date's simulated light curves plotted versus time for the SOR observer and the Moon-based observer are shown in the left and right plots of

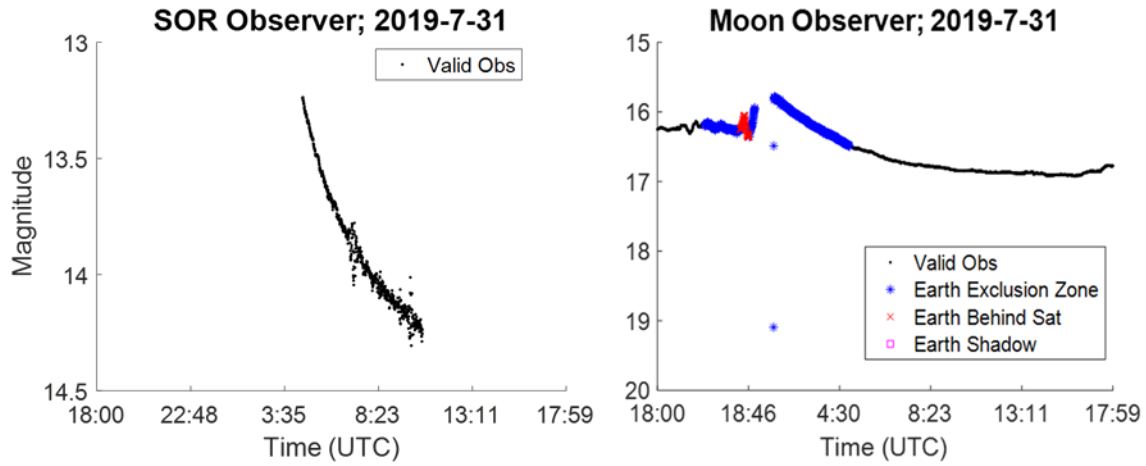


Fig. 8, respectively. While the satellite was close to perigee (around 22:50 UTC), neither sensor could view the target. As a result of the lack of observability, there is a gap or consecutive string of flagged observations in the light curves centered on 22:50 UTC. This is because the target was below the horizon for SOR or Earth was disrupting the Moon-based sensor's view of the target at this time. Note, the Moon observer's light curve (right plot) is cropped such that simulated magnitudes while the satellite was in Earth's shadow are not shown (these observations had magnitudes of about 40).

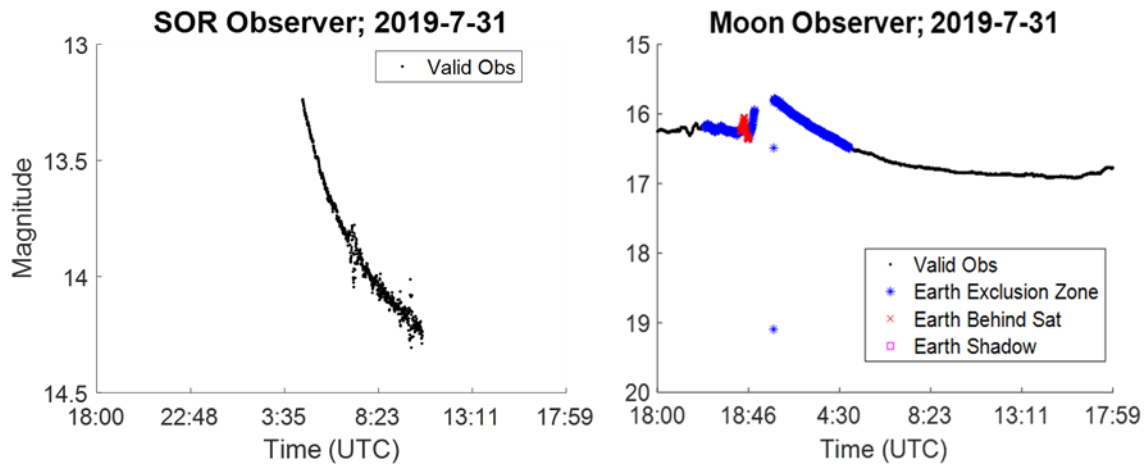
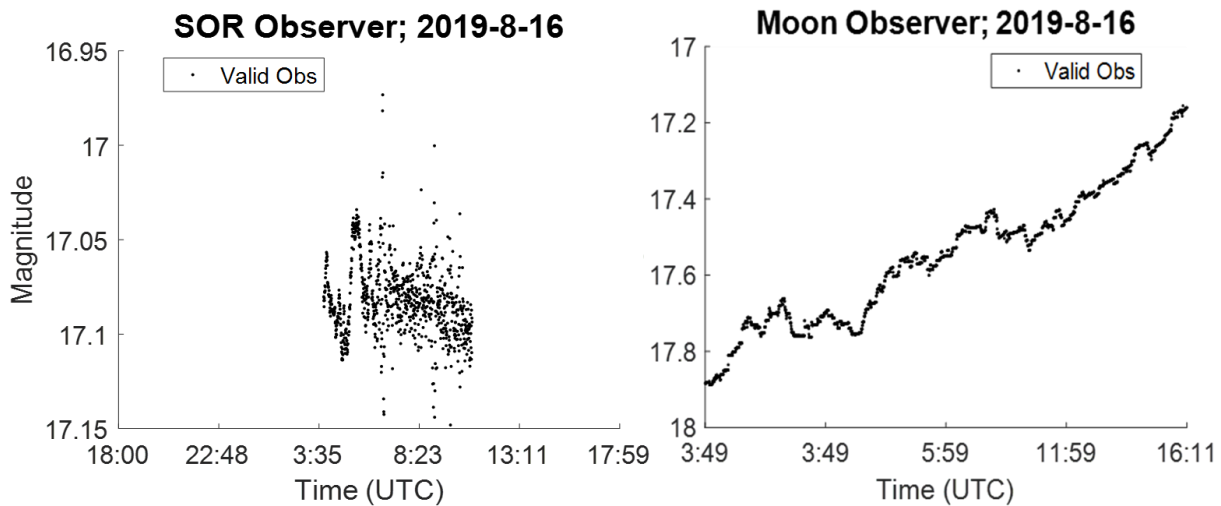


Fig. 8. Simulated Chandrayaan-2 Light Curves for SOR (Left) and Moon (Right) Observers for 31 Jul 2019

On 16 August 2019, the satellite was in transfer orbit F (refer to Table 1). This date's simulated light curves are plotted versus time for the SOR observer and the Moon-based observer and are shown in the left and right plots of

Fig. 9. Both light curves are relatively flat (i.e., have a small range of magnitude). This is most likely because the viewing angle was not changing much while the satellite is in transfer orbit. For example, the LPAs spanned



42.985° to 45.025° for SOR and 127.141° to 128.103° for the Moon observer during this night of observation.

Fig. 9. Simulated Chandrayaan-2 Light Curves for SOR (Left) and Moon (Right) Observers for 16 Aug 2019

On 22 August 2019, the satellite was in lunar orbit G (refer to Table 1). On this night, there was a waning gibbous Moon near third quarter. This date's simulated light curves plotted versus time, for both the SOR observer and the Moon-based observer, are shown in the left and right plots of Fig. 10. There is a gap in the light curve from the SOR sensor from about 19:00 to 5:50 UTC because the target was below the horizon. The remainder of the observations from the SOR sensor are flagged because the target was either within the Moon's exclusion zone or behind the Moon. Since the target orbited closer to the surface of the Moon over time, the target was completely unobservable from the SOR sensor on 22 August 2019. Gaps in the light curve for the Moon-based sensor are caused by the target falling below the horizon as it completes multiple revolutions around the Moon on 22 August 2019. The light curve contains a periodic pattern that repeats for each revolution. The multiple peaks and valleys in the light curve during each revolution are caused by the satellite performing yaw flips in order to stay Earth-nadir pointing. The dim observations (greater than 15 magnitudes) are caused by the satellite being backlit.

On 6 September 2019, the satellite was in lunar orbit J (refer to Table 1). On this night, the Moon was at first quarter. This date's simulated light curves plotted versus time for the SOR observer and the Moon-based observer are shown in the left and right plots of Fig. 11. The repetitive behavior in both Fig. 10 and Fig. 11 is due to the satellite completing multiple revolutions around the Moon. Gaps are present in each light curve because the target was passing below the horizon of the respective sensor. The target was again too close to the Moon on 6 September 2019 for the SOR sensor to observe the target at any point.

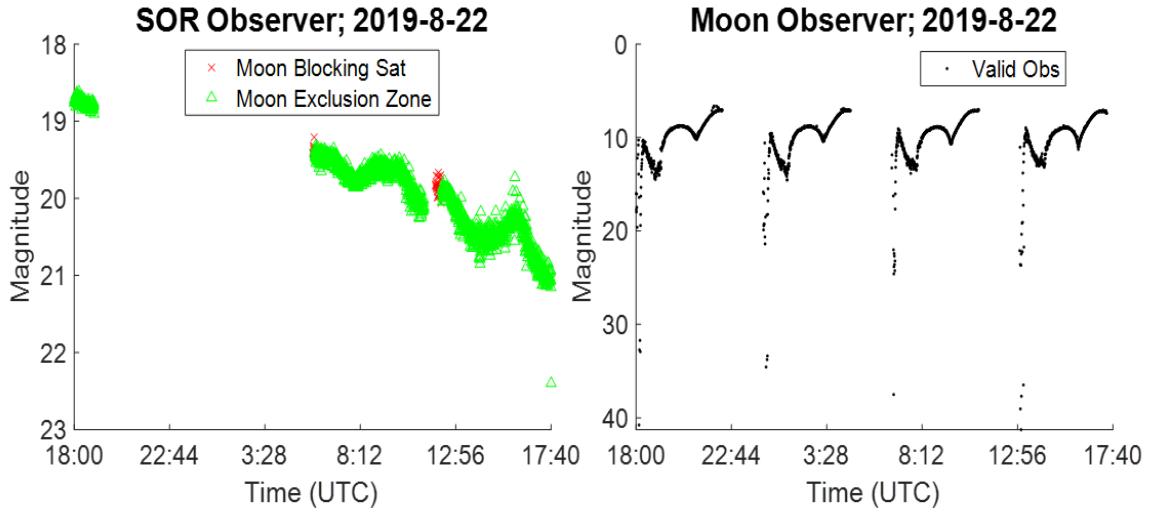


Fig. 10. Simulated Chandrayaan-2 Light Curves for SOR (Left) and Moon (Right) Observers for 22 Aug 2019

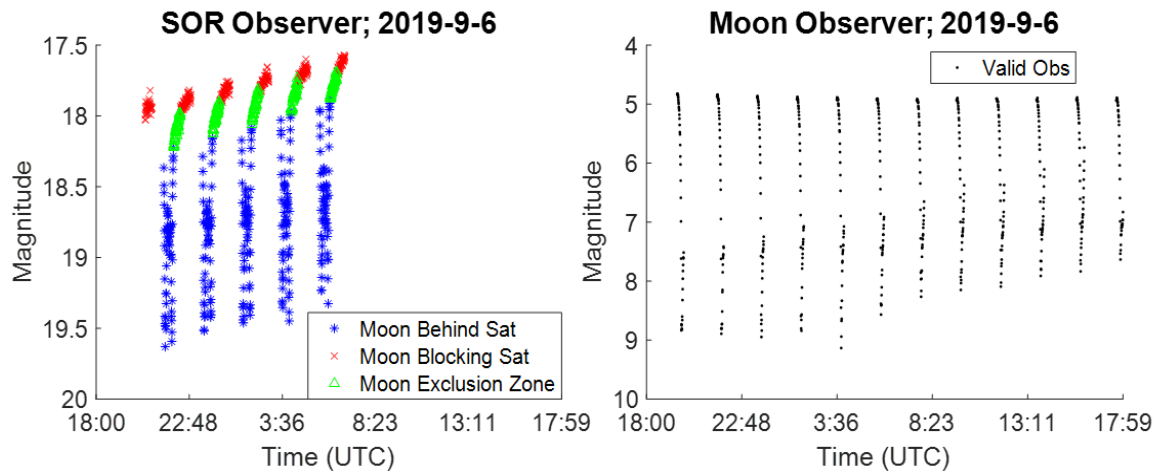


Fig. 11. Simulated Chandrayaan-2 Light Curves for SOR (Left) and Moon (Right) Observers for 6 Sep 2019

## 5. LEO TO L2 HALO TRAJECTORY

The trajectory of a satellite transitioning from LEO to a halo orbit around the Earth-Moon L2 Lagrange point was also simulated. The phases of the satellite's orbit are summarized in Table 2. This table includes the type, dates, inclination, and altitude from the surface of Earth for each phase of the orbit. For this scenario, we only used an Earth ground-based sensor located at SOR with two different models for the target: Galaxy-14 and Autonomous Nanosatellite Guardian for Evaluating Local Space (ANGELS). Both models are three-axis stabilized satellites with solar panels tracking the Sun and the bus facing Earth-nadir.

Table 2. Orbital Phases of Satellite's Trajectory

Type	Dates	INC (°)	Altitude (km)
<b>LEO</b>	11 – 13 Jan 2010	17	219
<b>Transfer</b>	13 – 20 Jan 2010	N/A	219 – 435,213
<b>L2 Halo</b>	20 Jan – 24 Feb 2010	N/A	389,258 – 463,702

To visualize the satellite's trajectory, the satellite's Earth Centered Inertial (ECI) coordinates are plotted with each orbital phase colored as in Table 2. The trajectory is plotted in Fig. 12. Due to the nature of the chosen LEO, the satellite could not be observed by SOR during the LEO phase. Because of this, the light curve began on 13 Jan 2010 while the satellite was in transfer orbit out to the Moon. Since the light curve simulations did not begin until the satellite was in mid-transfer orbit, that is where the plotted trajectory begins. Earth is represented by a blue dot (not to scale), and the Moon's trajectory is plotted as a light grey curve.

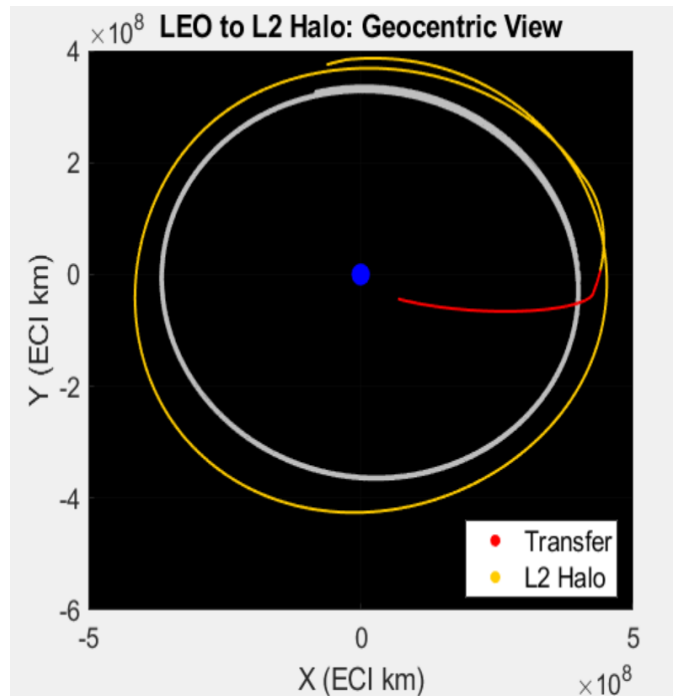


Fig. 12. Geocentric View of the Satellite's Trajectory

The light curves from each phase of the orbit are plotted separately to better understand how the orbit affects features of the light curve. Light curves for the ANGELS and Galaxy-14 satellite models from the SOR observer are plotted in a single figure. Since ANGELS is smaller than Galaxy-14, the light curves for the ANGELS model are consistently dimmer than the Galaxy-14 light curves.

During the transfer orbit, the satellite was traveling from LEO to the Moon. The light curves from the transfer orbit which span eight days (13-20 Jan 2010) are plotted in Fig. 13; only valid observations are displayed. During this period, the light curves became progressively darker from night to night as the satellite traveled further from Earth. The magnitudes were dim overall as the target was backlit by the Sun during the transfer orbit. There was increased variation present in the ANGELS light curve caused by more micro-glints in the SVST simulation for the ANGELS satellite model than for Galaxy-14.

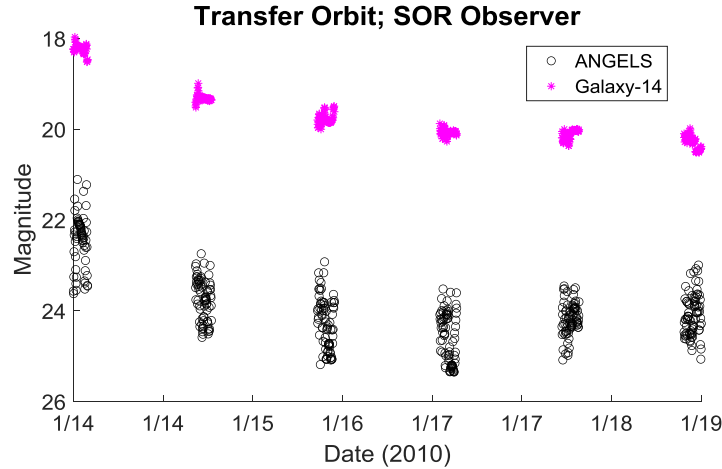


Fig. 13. Light Curves from Transfer Orbit Spanning 13-20 Jan 2010 for ANGELS and Galaxy-14 Models

To get a better sense of what the nightly light curves looked like during the transfer orbit, we plotted the light curve from the night of 15 Jan 2010 in Fig. 14. The light curves were relatively flat with no large peaks or valleys. This was most likely caused by the LPA not changing much during the transfer orbit. On the night of 15 Jan 2010, the LPA values ranged only from  $-134.251^\circ$  to  $-131.563^\circ$ . Like Fig. 13, the larger variation in the ANGELS light curve compared to the Galaxy-14 light curve is caused by several micro-glints occurring throughout the night for the ANGELS model.

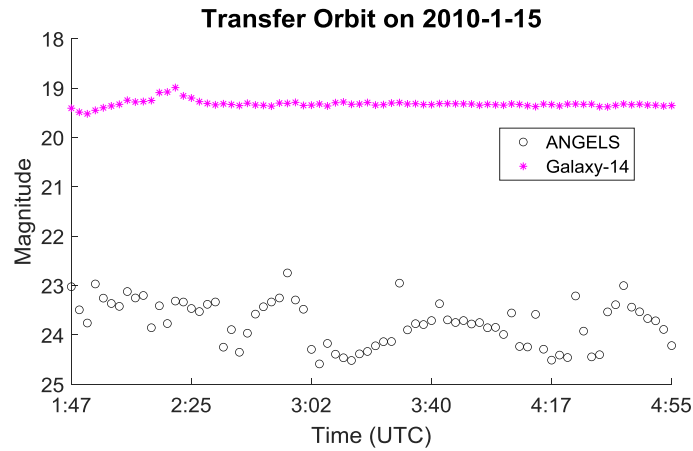


Fig. 14. Lightcurve during Transfer Orbit Taken the Night of 15 Jan 2010 for ANGELS and Galaxy-14 Models

After the satellite reached the Moon, it maneuvered to enter an L2 halo orbit. The satellite remained in this L2 halo orbit for two revolutions. The satellite's orbital period around L2 was approximately 14 days, resulting in the satellite being in its L2 halo orbit for about a month. This allowed us to observe light curves for each phase of the Moon. The simulated light curve for the extent of the L2 halo orbit is shown in Fig. 15; only valid observations are plotted. The full Moon and new Moon lunar phases are labeled on this figure.

During full Moon, the Moon and satellite were both near  $0^\circ$  LPA or minimum solar phase angle. As a result, there was a peak in brightness centered on the full Moon as the satellite approached  $0^\circ$  LPA, reached  $0^\circ$  LPA, then began to increase to larger LPA over the course of a couple weeks. There is a large gap at the full Moon caused by the satellite passing into the Moon's exclusion zone.

On the other hand, the observations centered on the new Moon are dimmer and noisier than observations taken around full Moon. This was caused by the Moon and satellite approaching high values of LPA. For example, at new Moon, the Moon's LPA is  $\pm 180^\circ$ . Both the Moon and the satellite are backlit by the Sun during this period. The gaps in observations around new Moon were caused by the sensor being in daylight while the Moon and the satellite were above the horizon from the sensor's point of view.

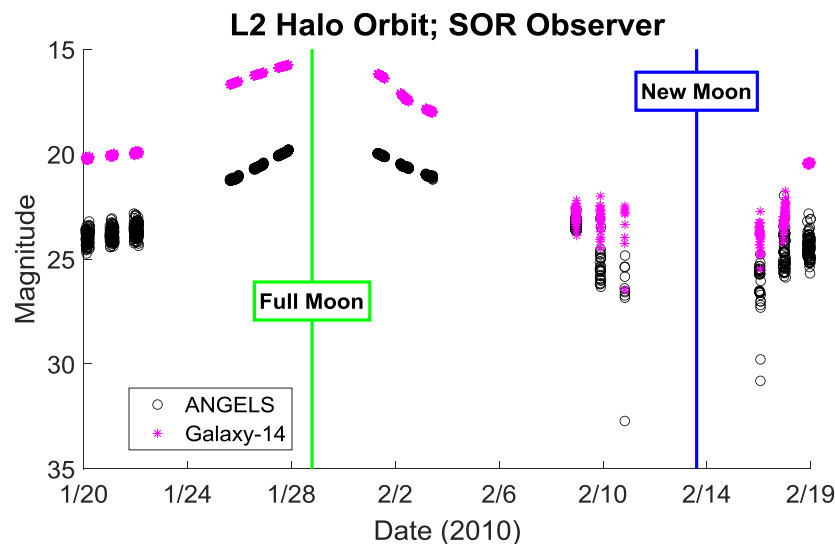


Fig. 15. Lightcurve during L2 Halo Orbit for ANGELS and Galaxy-14 Models with Full and New Moon Phases Labeled

## 6. SUMMARY AND CONCLUSIONS

The simulation of spacecraft in translunar, lunar, and cislunar orbits was accomplished using high fidelity solid models for typical satellite busses and using trajectories of past space experiments. When possible, the trajectories were reconstructed in GMAT. State information was ported to SVST to generate magnitudes. The light curves of RSOs while in these different orbits were studied. Table 3 contains the range of magnitude and altitude from Earth for each orbit simulated. These ranges of values were calculated only using valid, i.e., not flagged as physically or background excluded, observations. The types of exclusion are Moon shadow, Moon behind satellite, Moon blocking satellite, Moon exclusion zone, Earth behind satellite, Earth blocking satellite, Earth exclusion zone, Earth shadow, and Sun exclusion zone. The Chandrayaan-2 orbit with a Moon-based sensor resulted in the largest range of magnitudes and distances from the sensor. Alternatively, the Chandrayaan-2 orbit with a sensor at SOR had a relatively small range of magnitudes. This small range is the result of a vast majority of observations being flagged once the satellite entered lunar orbit. The results for the two LEO-L2 Halo orbit simulations are more similar to one another because the SOR sensor was used for both. However, we can see that the magnitude range for the Galaxy-14 target was generally brighter than the magnitude range for the ANGELS target. These differences in magnitude ranges are caused by the differences in size of the reflecting surfaces in the two target models.

The observability of cislunar objects can be affected by multiple factors, as evidenced by the sparseness of valid magnitudes. Though we did not take a limiting magnitude into account, the brightness of cislunar objects can become too dim to observe as a result of the inverse square law and the varying bidirectional reflectance of the complex models. The observability of cislunar objects is more greatly affected by lunar and solar exclusion zones than when objects are in orbits at or inside GEO. For an Earth ground-based observer, it was found that the cycle of a light curve increases in duration as the spacecraft moves from GEO to the Moon's sphere of influence due to the LPA changing more slowly as the object approaches the Moon. It was also found that the brightness variations change in character depending on the orbit. Translunar orbits have small variations in LPA causing the brightness to

vary less than when the object is in orbit around the Earth or the Moon. When objects in a lunar orbit are viewed by an Earth ground-based observer, LPA variation is less than in GEO but more than when in transfer orbit, so the brightness variations increase but by different amounts depending on the lunar phase.

Table 3. Range of Magnitude, Altitude, and Distance from Sensor per Simulated Orbit

Orbit	Target Model	Sensor Location	Magnitude Range	Altitude Range
<b>Apollo-6/Luna-1/5 day</b>	Galaxy-14	SOR	7.96 – 33.91	$2.9145 \times 10^6$ – $3.1912 \times 10^8$
<b>Chandrayaan-2</b>	Galaxy-14	SOR	9.57– 17.29	$1.1632 \times 10^7$ – $3.9764 \times 10^8$
<b>Chandrayaan-2</b>	Galaxy-14	Moon	0.29 – 37.65	$3.2144 \times 10^7$ – $3.99 \times 10^8$
<b>LEO-L2 Halo</b>	Galaxy-14	SOR	13.39 – 28.34	$1.5903 \times 10^8$ – $4.637 \times 10^8$
<b>LEO-L2Halo</b>	ANGELS	SOR	14.19 – 34.80	$1.5903 \times 10^8$ – $4.637 \times 10^8$

The results of our initial study of man-made objects in cislunar orbits have uncovered new aspects of the problem of monitoring objects beyond GEO and more study is warranted in order to specify top-level requirements of sensors capable of managing space traffic between the Earth and the Moon and maintaining SDA for safety in flight.

## REFERENCES

- [1] T. E. Payne, S. A. Gregory, A. V. Dentamaro, M. Ernst, J. Hollon, A. Kruchten and A. B. Chaudhary, "Development and Evaluation of New Methods for Estimating Albedo-area for Stable GEOs," in *The Advanced Maui Optical and Space Surveillance Technologies Conference*, Wailea, Maui, Hawaii, 2017 Sept 19-21.
- [2] E. Howell, "Chandrayaan-2: India's Orbiter-Lander-Rover Mission," 8 October 2019. [Online]. Available: <https://www.space.com/40136-chandrayaan-2.html>.
- [3] M. Wall, "Artemis Is Here:' Vice President Pence Stresses Importance of 2024 Moon Landing," 15 November 2019. [Online]. Available: <https://www.space.com/nasa-artemis-moon-program-mike-pence.html>.
- [4] A. Jones, "Chang'e-4 relay satellite enters halo orbit around Earth-Moon L2, microsatellite in lunar orbit," 14 June 2018. [Online]. Available: <https://spacenews.com/change-4-relay-satellite-enters-halo-orbit-around-earth-moon-l2-microsatellite-in-lunar-orbit/>.
- [5] "GSLV MkIII-M1 Successfully Launches Chandrayaan-2 spacecraft," Department of Space, 2019.
- [6] "Chandrayaan-2: All you need to know about India's 2nd Moon mission," The Times of India, 2019.
- [7] "Chandrayaan2 update: First earth bound maneuver," Department of Space, 2019.
- [8] "Chandrayaan2 update: Second earth bound maneuver," Department of Space, 2019.
- [9] "Chandrayaan2 update: Third earth bound maneuver," Department of Space, 2019.

- [10] "Chandrayaan2 update: Fourth earth bound maneuver," Department of Space, 2019.
- [11] "Chandrayaan2 update: Fifth earth bound maneuver," Department of Space, 2019.
- [12] "Chandrayaan-2 Successfully enters Lunar Transfer Trajectory," Department of Space, 2019.
- [13] "Chandrayaan-2 update: Lunar Orbit Insertion," Department of Space, 2019.
- [14] "Chandrayaan-2 update: Second Lunar Orbit Maneuver," Department of Space, 2019.
- [15] "Chandrayaan-2 update: Third Lunar bound Orbit Maneuver," Department of Space, 2019.
- [16] "Chandrayaan-2 update: Fourth Lunar Orbit Maneuver," Department of Space, 2019.
- [17] "Chandrayaan-2 update: Fifth Lunar Orbit Maneuver," Department of Space, 2019.
- [18] C. Mihos, "Orbital Energy," Case Western Reserve University, 23 July 2002. [Online]. Available: <http://burro.case.edu/Academics/Astr221/Gravity/orbenergy.htm>. [Accessed November 2019].